SPE 75691

Numerical Studies of Gas Production From Methane Hydrates

G.J. Moridis, SPE, Lawrence Berkeley National Laboratory, University of California

Copyright 2002, Society of Petroleum Engineers Inc.

This paper was prepared for presentation at the SPE Gas Technology Symposium held in Calgary, Alberta, Canada, 30 April–2 May 2002.

This paper was selected for presentation by an SPE Program Committee following review of information contained in an abstract submitted by the author(s). Contents of the paper, as presented, have not been reviewed by the Society of Petroleum Engineers and are subject to correction by the author(s). The material, as presented, does not necessarily reflect any position of the Society of Petroleum Engineers, its officers, or members. Papers presented at SPE meetings are subject to publication review by Editorial Committees of the Society of Petroleum Engineers. Electronic reproduction, distribution, or storage of any part of this paper for commercial purposes without the written consent of the Society of Petroleum Engineers is prohibited. Permission to reproduce in print is restricted to an abstract of not more than 300 words; illustrations may not be copied. The abstract must contain conspicuous acknowledgment of where and by whom the paper was presented. Write Librarian, SPE, P.O. Box 833836, Richardson, TX 75083-3836, U.S.A., fax 01-972-952-9435.

Abstract

EOSHYDR2 is a new module for the TOUGH2 general-purpose simulator for multi-component, multiphase fluid and heat flow in the subsurface. By solving the coupled equations of mass and heat balance, EOSHYDR2 can model the non-isothermal gas release, phase behavior and flow of fluids and heat under conditions typical of common natural hydrate deposits (i.e., in the permafrost and in deep ocean sediments) in complex formations, and can describe binary hydrocarbon systems involving methane.

EOSHYDR2 includes both an equilibrium and a kinetic model of hydrate formation and dissociation. The model accounts for up to four phases (gas phase, liquid phase, ice phase and hydrate phase) and up to nine components (hydrate, water, native CH_4 and CH_4 from hydrate dissociation, a second native and dissociated hydrocarbon, salt, water-soluble inhibitors and a heat pseudo-component). The mass components are partitioned among the phases. The thermophysical properties of the various mass components can be described at temperatures as low as –110 ^{o}C. Dissociation, phase changes and the corresponding thermal effects are fully described, as are the effects of salt and inhibitors. The model can describe all possible hydrate dissociation mechanisms, i.e., depressurization, thermal stimulation, salting-out effects and inhibitor-induced effects.

Results are presented for four test problems of increasing complexity that explore different mechanisms and strategies for production from typical CH_4-hydrate accumulations. The results of the tests indicate that CH_4 production from CH_4-hydrates could be technically feasible and has significant potential. In particular, thermal stimulation is capable of producing substantial amounts of hydrocarbons, and its effectiveness can be enhanced when coupled with depressurization and the use of inhibitors.

Introduction

Gas hydrates are solid crystalline compounds in which gas molecules are encaged inside the lattices of ice crystals. These gases are referred to as guests, whereas the ice crystals are called hosts. Of particular interest are hydrates in which the gas is a hydrocarbon. Under suitable conditions of low temperature and high pressure, a hydrocarbon gas M will react with water to form hydrates according to

$$M + N_H H_2O = M \bullet N_H H_2O,$$

where N_H is the hydration number.

Vast amounts of hydrocarbons are trapped in hydrate deposits[1]. Such deposits exist where the thermodynamic conditions allow hydrate formation, and are concentrated in two distinctly different types of geologic formations where the necessary low temperatures and high pressures exist: in the permafrost and in deep ocean sediments. The lower depth limit of hydrate deposits is controlled by the geothermal gradient.

Current estimates of the worldwide quantity of hydrocarbon gas hydrates range between 10^{15} to 10^{18} m^3. Even the most conservative estimates of the total quantity of gas in hydrates may surpass by a factor of two the energy content of the total fuel fossil reserves recoverable by conventional methods[1]. The magnitude of this resource could make hydrate reservoirs a substantial future energy resource. While current economic realities do not favor gas production from the hydrate accumulations, their potential clearly demands evaluation.

The majority of naturally occurring hydrocarbon gas hydrates contain CH_4 in overwhelming abundance. Simple CH_4-hydrates concentrate methane volumetrically by a factor of 164, and require less than 15% of the recovered energy for dissociation. Natural CH_4-hydrates crystallize mostly in the I structure, which contains 46 H_2O molecules per unit cell. They have a N_H ranging from 5.77 to 7.4[1], with N_H = 6 being the average

hydration number and N_H = 5.75 corresponding to complete hydration.

There are three main methods of hydrocarbon recovery from gas hydrates: (a) thermal stimulation[2], in which gas release is effected by heating the hydrate above the dissociation temperature at a given pressure, (b) depressurization[3], in which the gas release is achieved by lowering the pressure below that of the hydrate stability, and (c) 'inhibitor' injection[4] in which the hydrocarbon is produced after the injection of substances (e.g., brines, alcohols) that destabilize the hydrate. Combinations of these methods can also be used.

Only two numerical codes have been developed for the simulation of gas production from dissociating hydrates. Drenth and Swinkels[5] developed a four-component, three-phase numerical model for the equilibrium dissociation of binary hydrates in marine environments. An improved version of the code with advanced thermodynamics was later developed by the same authors, who provided an in-depth discussion of the challenges facing production from gas hydrates and identified knowledge gaps in numerical simulation of gas production from hydrate dissociation[6].

Moridis *et al.*[7] developed EOSHYDR, a TOUGH2[8,9] module for the simulation of dissociating simple methane hydrates under equilibrium and kinetic conditions in both permafrost and marine accumulations. In this paper, I discuss the development and performance of EOSHYDR2, a new module for the simulation of reservoir fluid flow and behavior in hydrate accumulations. EOSHYDR2 can model any combination of hydrate dissociation mechanism. It describes the non-isothermal formation or dissociation of simple CH_4- or composite CH_4- and $C_\nu H_{2\nu+2}$-hydrates using accurate thermophysical properties and the most recent information on the parameters of equilibrium or kinetic dissociation.

Governing Equations

Depending on the thermodynamic state of the system, the amount of hydrate created or CH_4 released is determined from the reaction

$$CH_4 \cdot N_m H_2O \leftrightarrow CH_4(\text{gas}) + N_m H_2O \ (\text{liquid or ice}) \quad \text{.....(1)}$$

where N is the hydration number, and the subscript m denotes methane. In addition to simple CH_4-hydrates, EOSHYDR2 allows the study of composite hydrates involving a second hydrocarbon that can be ethane, propane, or butane (iso- or normal-). Such hydrocarbons exist in practically all natural hydrates and can play a significant role in their nucleation and behavior. The reaction describing the formation/hydration of the second hydrocarbon in the composite hydrate is

$$C_\nu H_{2\nu+2} \cdot N_\nu H_2O \leftrightarrow C_\nu H_{2\nu+2}(\text{gas}) + N_\nu H_2O \ (\text{liquid or ice}) \quad \text{....(2)}$$

where the subscript ν denotes the $C_\nu H_{2\nu+2}$ hydrocarbon (ν=2,3, or 4). The composite hydrate is then represented as

$$\chi_m[CH_4.N_m H_2O]\ \chi_\nu[C_\nu H_{2\nu+2}.N_\nu H_2O],$$

where χ is the mole fraction of the different hydrocarbon. Obviously, $\chi_m+\chi_\nu = 1$. Although χ_m often exceeds 95% in natural hydrates, the other hydrocarbon constituent of the composite hydrate cannot be ignored because it can have a significant effect on the equilibrium conditions of the system[1].

A non-isothermal hydrate system can be fully described by the appropriate mass balance equations and an energy balance equation. Following the convention of TOUGH2[8,9], the following components are considered in EOSHYDR2:

$w(*)$	for water
$m(*)$	for CH_4
ν	$C_\nu H_{2\nu+2}$
$h(*)$	for the hydrate
s	for salt in water
i	for inhibitors (e.g., alcohols)
$\theta(*)$	for heat

The components marked by an asterisk are the minimum necessary for a hydrate simulation. Note that it is possible to replace m by the pair $m1$ and $m2$, which represent the native and hydrate-derived methane (hereafter referred to as 'dissociated' CH_4), respectively. The same can be done with the component ν. This allows accurate tracking of the dissociation contribution to gas production in the presence of native gas(es). Thus, in its most complex realization, EOSHYDR2 can track a total of N_κ = 9 separate components.

Mass balance in every subdomain (gridblock) n into which the flow domain is subdivided by the integral finite difference method of TOUGH2[8,9] dictates that

$$\frac{d}{dt}\int_{V_n} M^\kappa dV = \int_{\Gamma_n} F^\kappa \cdot \mathbf{n}\, d\Gamma + \int_{V_n} q^\kappa dV \quad \text{.....(3)}$$

There are four possible phases β: an aqueous phase ($\beta = A$), a gaseous phase consisting of CH_4, $C_\nu H_{2\nu+2}$ and water vapor ($\beta = G$), a solid hydrate phase ($\beta = H$), and a solid ice phase ($\beta = I$). The hydrate is treated as an immobile component (albeit degenerate) and a phase, and thus it may reduce by one the number of equations to solve.

Accumulation Terms

The mass accumulation terms of the fluids in equation (3) are given by

$$M^w = \sum_{\beta \equiv A,G,I} \phi S_\beta \rho_\beta X_\beta^w + M_H^w$$
$$M^{m,v} = \sum_{\beta \equiv A,G,I} \phi S_\beta \rho_\beta X_\beta^{m,v} + M_H^{m,v} \quad \text{.....(4)}$$

The rightmost terms in equation (4) are pseudostorage terms, describe the amount of water and hydrocarbons stored in the hydrate, and, under equilibrium conditions, they are given by

$$M_H^{w,m,v} = \phi S_H \rho_H X_H^{w,m,v}, \text{ where}$$
$$X_H^w = \frac{(\chi_m N_m + \chi_v N_v) W_w}{W_h}, \quad X_H^m = \frac{\chi_m W_m}{W_h}, \quad X_H^v = \frac{\chi_v W_v}{W_h} \quad \text{.....(5)}$$

Under kinetic conditions, there is no pseudostorage.

The mass accumulation terms of the salt and inhibitor involve the aqueous phase only, and are given by

$$M^{s,i} = \left[\phi S_A + (1-\phi)\rho_R K_d^{s,i}\right] \rho_B X_A^{s,i} \quad \text{.....(6)}$$

Implicit in equation (6) is the assumption of a linear equilibrium sorption of the component $\kappa = s,i$ onto the rock. Volume and mass balance dictate that, in each control volume,

$$\sum_{\beta \equiv A,G,I,H} S_\beta = 1 \quad \text{and} \quad \sum_\kappa X_\beta^\kappa = 1 \quad \text{for each phase } \beta \quad \text{.....(7)}$$

Because of the prevailing conditions during hydrate formation/dissociation, the hydrocarbons must be treated as real (rather than ideal) gases. Thus, the density of the gas phase is computed as

$$\rho_G = \frac{P_G \sum_\kappa Y_G^\kappa W_\kappa}{ZRT}, \quad \text{.....(8)}$$

where $\kappa = m$ (or *m1,m2*), v (or *v1, v2*), *w, i* in the gas phase.

Salts inhibit hydrate formation because of the much stronger affinity of water for ions than to hydrate structures, and because of a decrease in the solubility of potential hydrate guest molecules in water[1]. The effect of salts on hydrate dissociation is quantified through the change of the equilibrium dissociation temperature at a given pressure. The hydrate formation temperature in the presence of salt, T_s, is obtained from the equation[1]

$$T_s = \left[\frac{1}{T_w} - \frac{n_H \Delta H^f}{\Delta H^0}\left(\frac{1}{273.15} - \frac{1}{T_{fs}}\right)\right]^{-1} \quad \text{.....(9)}$$

Inhibitors such as alcohols bond preferentially with water molecules through hydroxyl groups and tend to organize water in solvent clusters, thus competing with the hydrate for guest and host molecules. The effect of such inhibitors is a depression of the hydrate equilibrium temperature, which is computed from the Nielsen and Bucklin[10] equation as

$$\Delta T = -C_i \ln(1 - x_A^i) \quad \text{.....(10)}$$

where C_i is an inhibitor-specific constant.

The heat accumulation term includes contributions from the rock matrix and all the phases, and is given by the equation

$$M^\theta = (1-\phi)\rho_R C_R T + \sum_{\beta \equiv A,G,H,I} \phi S_\beta \rho_\beta u_\beta \quad \text{.....(11)}$$

The terms u_A and u_G are obtained from

$$u_A = \sum_{\kappa \equiv w,m,v,s,i} X_A^\kappa u_A^\kappa \quad \text{and} \quad u_G = \sum_{\kappa \equiv w,m,v} X_G^\kappa u_G^\kappa, \quad \text{.....(12)}$$

The solubility of hydrocarbons in the aqueous phase is small, but for consistency their heat of dissolution is accounted for in the heat balance equation. On the other hand, the specific internal energy of the gaseous phase is a very strong function of composition. Note that Joule-Thompson effects are fully accounted for in EOSHYDR2.

Flux Terms

The mass fluxes of water and hydrocarbons include contributions from the aqueous and gaseous phases, i.e.,

$$F^\kappa = \sum_{\beta \equiv A,G} (\mathrm{F}_\beta^\kappa + \mathrm{J}_\beta^\kappa) \quad \text{.....(13)}$$

The contributions of the two solid phases *(β=H,I)* to the fluid fluxes are zero. The term $\mathbf{J}_\beta^\kappa$ is the diffusive mass flux of component κ in phase β, and is described by

$$\mathbf{J}_\beta^\kappa = -\phi S_\beta \underbrace{(\phi^{1/3} S_G^{7/3})}_{\tau_G} \mathbf{D}_\beta^\kappa \rho_\beta \nabla X_\beta^\kappa, \quad \text{.....(14)}$$

where κ=*w, m* (or *m1,m2*), v (or *v1, v2*), τ_G is the gas tortuosity computed from the Millington and Quirk[11] model, and $\mathbf{D}_\beta^\kappa$ is the hydrodynamic dispersion tensor that is described by

$$\mathbf{D}_\beta^\kappa = \mathrm{D}_{\beta,T}^\kappa \mathbf{I} + \frac{\mathrm{D}_{\beta L}^\kappa - \mathrm{D}_{\beta T}^\kappa}{\upsilon^2} \mathbf{v}\,\mathbf{v}$$
$$\mathrm{D}_{\beta,L}^\kappa = d_\beta^\kappa + \alpha_L \upsilon, \quad \mathrm{D}_{\beta,T}^\kappa = d_\beta^\kappa + \alpha_T \upsilon \quad \text{.....(15)}$$

Note that the full hydrodynamic dispersion is used only for $\kappa = s,i$, while fluxes from molecular diffusion are accounted for in the gas phase and can be included in the computations of transport of the dissolved hydrocarbons.

For the aqueous phase,

$$\mathbf{F}_A^\kappa = X_A^\kappa \mathbf{F}_A, \qquad \mathbf{F}_A = -k\frac{k_{rA}\rho_A}{\mu_A}(\nabla P_A - \rho_A \mathbf{g}) \qquad \text{……(16)}$$

with the phase flux $\mathbf{F}_A$ being described by Darcy's law. The aqueous pressure P_A is given by

$$P_A = P_G + P_c, \qquad P_G = P_G^m + P_G^w + P_G^\nu \qquad \text{……...……(17)}$$

In EOSHYDR2 simulations, relative permeabilities and capillary pressures P_c can be estimated using one of the several three-phase models available to the TOUGH2 family of codes[8,9].

The mass flux of the gaseous phase (β=G) incorporates advection and diffusion contributions, and is given by

$$\mathbf{F}_G^\kappa = -k\left(1+\frac{b}{P_G}\right)\frac{k_{rG}\rho_G}{\mu_G} X_G^\kappa (\nabla P_G - \rho_G \mathbf{g}) + \mathbf{J}_G^\kappa \qquad \text{……...…….(18)}$$

The heat flux accounts for both conduction and convection, and is given by

$$\mathbf{F}^\theta = -\{(1-\phi)K_R + \phi[S_H K_H + S_I K_I + S_A K_A + S_G K_G]\}\nabla T + \sum_{\beta\equiv A,G} h_\beta \mathbf{F}_\beta, \qquad \text{…….…….(19)}$$

in which the phase-specific enthalpy is computed from

$$h_A = \sum_{\kappa\equiv w,m,\nu,s,i} X_A^\kappa h_A^\kappa \quad \text{and} \quad h_G = \sum_{\kappa\equiv w,m} X_G^\kappa h_G^\kappa \qquad \text{..……..(20)}$$

Note that the heat of dissociation ΔH^0 is incorporated into the specific internal energy and specific enthalpy of equations (12) and (20), respectively.

Source and Sink Terms

In the equilibrium model, injection of a fluid into the reservoir can occur at mass rates q^κ ($\kappa = w,m,\nu,s,i$), while removal of the various mass components is described by

$$q^\kappa = \sum_{\beta\equiv A,G} X_\beta^\kappa q_\beta, \quad \kappa \equiv w,m,\nu,s,i \qquad \text{……......……..(21)}$$

In the kinetic model, the additional sink/source terms corresponding to hydrate dissociation and release of hydrocarbons and H_2O must be accounted for. The source terms for the hydrocarbons thus become $q^\kappa+Q^\kappa$ (κ=m,ν), where the generation rate Q^κ is determined from the hydrate kinetic reaction model of Kim *et al.*[12] as

$$Q^\kappa = \chi_\kappa W_\kappa A_\kappa k_\kappa \exp(\frac{\Delta E^\kappa}{RT})[f_{e\kappa}(T) - f_\kappa], \quad \kappa \equiv m,\nu \qquad \text{……..(21)}$$

Values of the kinetic reaction parameters for a number of hydrocarbons can be found in Kim *et al.*[12] and Clarke and Bishnoi[13,14].

The rate of generation of water is given by

$$Q^w = \sum_{\kappa\equiv m,\nu} \chi_\kappa N_\kappa W_w A_\kappa k_\kappa \exp(\frac{\Delta E^\kappa}{RT})[f_{e\kappa}(T) - f_\kappa] \qquad \text{……..…….(22)}$$

while the rate of dissociation of the hydrate is determined from Q^h=-$(Q^w+Q^m+Q^\nu)$. Note that the available information on the kinetic parameters of dissociation was obtained from laboratory studies involving synthetic hydrates. It is not known if these are representative of dissociation in natural hydrate systems. Thus, caution should be exercised in the application of the kinetic model.

Under equilibrium conditions, the rate of heat removal or addition includes contributions of (a) the heat associated with fluid removal or addition, as well as (b) direct heat inputs or withdrawals (e.g., microwave heating), and is described by

$$q^\theta = q_d + \sum_{\beta=A,G} h_\beta q_\beta. \qquad \text{……..……(23)}$$

Under kinetic conditions, this equation is extended to account for the heat of dissociation, thus becoming

$$q^\theta = q_d + \sum_{\beta=A,G} h_\beta q_\beta + Q^h \Delta H^0 \qquad \text{……...……(24)}$$

Note that equation (23) applies to the subdomains V_n where fluids and heat are produced or injected, while equation (24) applies to all such subdomains V_n in addition to all subdomains where hydrate dissociation or formation occurs.

Phase Equilibrium and Thermophysical Properties

Of particular interest are the pressures and temperatures of the L_w-H-V and I-H-V three-phase lines in the H_2O-CH_4 diagram, which delineate the limits to hydrate formation. Using the equilibrium dissociation option, dissociation of the simple CH_4 hydrate is treated in a manner akin to a phase change of a

pure substance (e.g., water vaporization), and is determined from the equilibrium pressure and temperature relationship. The relationship between the equilibrium P and T in EOSHYDR can be obtained from two sources. The first is the regression equation of Kamath[15]

$$P_e = \exp\left(e_1 + \frac{e_2}{T}\right), \quad \text{.....(25)}$$

where

$$e_1 = \begin{cases} 38.980 \\ 14.717 \end{cases} \text{ and } e_2 = \begin{cases} -8533.80 & \text{for } 0^oC \geq T \geq 25^oC \\ -1886.79 & \text{for } -25^oC \geq T \geq 0^oC \end{cases}$$

The second source is a general regression expression derived from the data from several researchers reported by Sloan[1]. The two relationships and their range are shown in Figure 1. Note that EOSHYDR2 includes a model to describe hysteresis (due to metastability) between the heating (dissociation) and cooling (formation) P-T equilibrium curves, but its accuracy cannot be verified because no relevant data are available for verification.

For composite hydrates, distribution of the hydrocarbons in the gas and hydrate phases are determined from the equilibrium distribution coefficient ($K_{vs\kappa}$ value) method of Carson and Katz[16]. The hydrocarbon-specific $K_{vs\kappa}$ is defined as $K_{vs\kappa}=y_\kappa/\chi_\kappa$, where χ_κ is the mole fraction of component κ in the water-free vapor. Partitioning of the various gases is determined iteratively, making use of the requirement that at equilibrium $\Sigma y_\kappa/K_{vs\kappa}=1$. Thus, dissociation of composite hydrates results in continuously changing hydrate stoichiometry.

The properties of the real gas mixtures (compressibility, fugacities, and enthalpy deviations from ideal gas behavior) in EOSHYDR2 are computed from the Peng-Robinson equation of state using the interaction parameters of Soreide and Witson[17]. The water thermodynamic tables available in TOUGH2[8,9] were extended to cover the 160 ^{o}K (-110 ^{o}C) to 773 ^{o}C (500 ^{o}C) range. This range allows investigation and analysis of hydrate behavior under extreme laboratory conditions. Some gas transport properties were obtained from Vargaftik[18], while the Pressure-Temperature-Composition (P-T-X) diagrams of Kobayashi and Katz[19] were also used. The viscosity of the real gas mixtures is computed using the method of Chung *et al.*[20]. In the absence or reliable data, hydrocarbon solubility in the vicinity of the hydration point is computed from the equality of fugacities of the gas and aqueous phases.

There are limited data on the temperature dependence of heat of dissociation ΔH^0, which is often taken as constant over small temperature ranges. In EOSHYDR2, ΔH^0 under three-phase conditions (L_w-H-V and I-H-V) can be computed from either the simple equation of Kamath[15] as $\Delta H^0 = C_1 + C_2/T$ (where C_1 and C_2 are constants), or can be determined from the Clausius-Clapeyron equation

$$\Delta H^0 = zRT^2 \frac{d\ln P}{dT} \quad \text{.....(25)}$$

using the gas compressibility Z and the known $d\ln P/dT$ of the hydrate equilibrium relationship (from the regression curve, see Figure 1). Figure 2 shows the ΔH^0 relationships from both equations. For comparison, Figure 2 includes the laboratory measurements of ΔH^0 reported in Sloan[1].

Test Problems

Various preliminary test runs indicated that EOHYDR2 was capable of predicting the formation and dissociation of simple CH_4 hydrates at the known equilibrium pressures and temperatures shown in Figure 1. Additionally, EOSHYDR2 could accurately (compared to laboratory data and the predictive equations of Sloan[1]) predict the hydrocarbon composition in the gas phase for a known composition of the binary hydrate (and vice versa).

Test Problem 1

Test Problem 1 involves the depressurization-induced release of CH_4 in a reservoir containing stratified layers of CH_4 gas and hydrate deposits under permafrost conditions. Figure 3 and Table 1 show a schematic of the reservoir and the reservoir properties, respectively. Gas is produced in a single well completed throughout the gas zone. The well is located at the center of the reservoir, and its production rate is constant at 0.81944 m^3/s (2.5 MMFCD).

The problem was first studied by Holder *et al.*[3], who solved the uncoupled pressure and temperature equations by using a 2-D grid for pressure calculations and a 3-D grid for temperature calculations. In their approach, the heat transferred to the interface (due to the temperature gradient) was used for the hydrate dissociation, and there was no energy balance based on the existing phases and their enthalpies.

Because of the radial symmetry of the problem and the need to have a higher definition in the vicinity of the well bore, the system was simulated using a 2-D cylindrical grid. The reservoir radius was r = 567.5 m, and its thickness was 30.5 m (100 ft) equally distributed between the hydrate layer and the free gas zone. These dimensions result in a reservoir with a volume identical to the cartesian system of Holder *et al.*[3].

The system was discretized in 80x40 = 3,200 gridblocks in (r,z). Using the equilibrium model, a total of 12,800 coupled equations were solved simultaneously (the dissociated gas was tracked separately). This discretization provided gridlocks as small as 0.1 m in Δz, while the radial discretization followed a logarithmic distribution. This discretization provided substantial detail near the wellbore. The wellbore itself was simulated by the first column of gridblocks at the origin of the system, in which the vertical permeability was practically infinite

compared to the reservoir permeability of 4.3425×10^{-14} m^2 (44 md). The horizontal permeability of the wellbore gridblocks was zero in the hydrate layer and equal to the reservoir permeability in the free gas zone. The production rate was assigned to the top wellbore gridblock.

Two cases were tested. In Case 1, the initial hydrate saturation in the hydrate zone was $S_H = 1$, which results in zero initial fluid permeability in this region. However, after the beginning of dissociation, the permeability of gas and released water are no longer zero, and they are determined from the fluid saturations and the relative permeability curve. In Case 2, $S_G = 0.7$ and $S_A = 0.3$. For the relative permeability and capillary pressure curves, the Parker *et al.*[21] model was used.

Figure 4 shows the cumulative contribution of hydrate dissociation to the total gas production as a function of production times. Compared to the Holder *et al.*[3] results, our simulation indicates a much higher contribution of dissociated gas in Case 1 (which corresponds to the Holder *et al.*[3] conditions). The difference is attributed to the fact that in our model a gas phase emerges in the hydrate zone, which keeps expanding as the dissociation continues and the released water drains. Additionally, the water released through decomposition occupies a volume 13% smaller than the corresponding hydrate, thus further increasing S_G. In Case 2, the cumulative contribution of dissociated gas is higher due to the higher permeability to gas movement, which allows dissociation over a larger volume of hydrate.

Figure 5 shows the vertical temperature profiles at a distance r = 0.15 m from the wellbore. In Case 1, the maximum temperature decrease is 8.23 K, occurs at z =-14.6 m, i.e., 0.4 m above the initial interface, and is significantly larger than the 1.2 ^oK drop reported by Holder *et al.*[3]. The differences are attributed to the reasons mentioned above, as well as to the much finer discretization in the vicinity of the well bore. In Case 2, the maximum temperature decrease is 7.11 ^oK and occurs 0.6 m above the initial interface. The differences between Cases 1 and 2 are attributed to the higher gas permeability in Case 2.

Figure 6 shows the evolution over time of the pressure at the wellbore gridblock immediately below the initial interface (at r = 0.05 m and z =-15.05 m). The pressure in Case 1 is lower than the Holder *et al.*[3] results, but the difference is rather small. It appears that the reason for the similarity of the answers is that the finer discretization and higher dissociation in our model produce roughly the same results as the coarser discretization and lower dissociation of the Holder *et al.*[3] model. The pressures in Case 2 are larger than those in Case 1 due to the higher permeability (and, consequently, the higher hydrate dissociation) of the gas phase.

Test Problem 2

Test Problem 2 involves the depressurization-induced release of CH_4 in a reservoir of simple CH_4 hydrates and salt water (no free gas phase), i.e., under conditions of ocean sediments. The distribution of water and hydrate was uniform throughout the reservoir, with initial $S_A = S_H = 0.5$ and $S_G = 0$. The reservoir dimensions, properties, and the initial conditions were the same as in Problem 1. The properties and concentration of seawater were used in this simulation. Fluids were produced by setting the pressure at the wellbore gridblock at z = -14.95 m, i.e., immediately above the interface, constant at 1.7237×10^7 Pa (2500 psi), and were distributed in the production stream according to their mobilities.

The cumulative gas production over time (shown in Figure 7 is roughly proportional to the square root of time, and reaches the level of 4.114×10^7 m^3 (1.453×10^9 ft^3) after a year of production. The reason for this substantial level of production appears to be the very low compressibility of water. The temperature distribution along z at r = 0.15 m (Figure 8) tends to support this thesis, as the temperature decrease is larger and more extended than in Problem 1. Although this is a simplified example, the results are encouraging for CH_4 production from hydrates in ocean sediments.

Test Problem 3

Test Problem 3 simulates the release of CH_4 through a thermal stimulation process in a reservoir of CH_4 hydrates and free CH_4 gas phase, i.e., under permafrost conditions. The problem simulated here is the frontal sweep production system discussed by McGuire[3], which is similar to the steam flooding process in heavy-oil reservoirs. The frontal sweep method involves wells arranged in a five-spot pattern (Figure 9). The injected fluid was hot water because the parametric study of McGuire[3] indicated that when steam is injected, the amount of produced gas was less than the estimated fuel consumption. This problem involves a combination of thermal stimulation (at the injection well) with depressurization (at the production well), and appears to be superior to simple depressurization because of the combined effect of the two dissociation methods in addition to the substantial advantage of thermal stimulation over depressurization (as attested to by the P-T equilibrium curve). Note that it is practically impossible to have a pure thermal stimulation process because pressure changes at the wells (during injection and production) and the significant pressure increase during dissociation affect the dissociation (though less than temperature) and have to be accounted for.

Because of symmetry, only 1/4 of the basic pattern needs to be modeled. The side of the basic square was 500 m, and the thickness of the reservoir was 30.5 m (100 ft). The domain was discretized in 20x20x20 = 8,000 gridblocks in (x,y,z), resulting in a uniform gridblock size of 25m x 25 m x1.525 m and a total of 32,000 equations (equilibrium model). The injection well was completed in the bottom half of the reservoir, while the production well was completed in the top half. The reservoir porosity was 0.25, and initially $S_H = 0.6$ and $S_A = 0.4$. All other

reservoir properties and the initial pressure and temperature were the same as in the Test Problem 1. The change from the problem described by McGuire (1981) was made because it would be impossible to establish flow in a system fully saturated with hydrates (i.e., when $S_H = 1$).

Pure water and brine (15% in NaCl) at 333.15 ^oK were injected at the rate of 0.055 kg/s used in the McGuire[3] study. Figure 10 shows the cumulative CH_4 production over a year of injection and gas production. At the end of the year, the amount of CH_4 ($2.36x10^7$ m^3) produced with pure water is substantially smaller than the McGuire[3] estimate ($4.9636x10^7$ m^3) for the same injection temperature. This was expected because of the smaller amount of available hydrate (the McGuire model was not a porous medium model) and the resistance to flow that the hydrates present[3]. The produced gas, however, is well above the ($1.41 x10^7 m^3$) level necessary to cover the fuel consumption for heating the injected water.

The cumulative CH_4 production when brine is injected is larger than the corresponding CH_4 production with pure water injection, but the effect of the salt appears moderate to small. This is attributed to the continuous dilution of the advancing salt front by the large amounts of water released during the hydrate dissociation.

Figure 11 shows the temperature distribution along the line connecting the producing and injection well at z = -16 m from the reservoir top at t = 1 year. The curve exhibits a region of temperature decline associated with the advancing hot water front. A second region with declining temperatures below the initial temperature level is evident in the vicinity of the production well, and is attributed to the inevitable depressurization process as fluids are withdrawn.

Test Problem 4

This problem involves production from a suboceanic hydrate-capped gas reservoir, and is very similar to the one discussed by Swinkels and Drenth[6]. Some information on the reservoir depth and geology is provided in Figure 12. A quarter of the domal structure is simulated using a 30x30x40 unequally spaced grid that resulted in a total of 216,000 equations. The permeability of the hydrate-free rock is 200 mD, the initial pressure is 100 bars, the porosity is 0.2, and the geothermal gradient is 0.03 $^oK/m$. Specifics on the reservoir conditions and parameters can be found in Swinkels and Drenth[6]. The free gas below the hydrate layer is composed of 80% methane and 20% ethane. In this simulation, the dissociated and native hydrocarbons were tracked separately. Gas was produced through a 500 m-long horizontal well, of which 450 m were perforated. This is sufficient to allow a gas flow of 10^6 m^3/day.

Initialization of the model requires that the temperature and pressure profile vs. depth and the phase behavior of the hydrate be consistent. This was accomplished by first determining the hydrate composition for the pressure and temperature distributions along the profile from the ocean floor to the bottom of the hydrate layer, assigning these distributions to the reservoir at the appropriate depths, and running the system to equilibrium (which required about 10^5 years).

The results of the simulation are shown in Figures 13 to 17, all of which show data along the vertical axis that passes through the well midpoint. The pressure distribution in Figure 13 shows that, despite a very substantial pressure drop in the free gas zone, the hydrate remains competent and relatively impermeable (as indicated by the invariable pressure distribution above the base of the hydrates). This is consistent with expectations because hydrates can reduce drastically the permeability of the pore space they occupy and are effective gas caps.

The cooling effect of hydrate dissociation is evident in Figure 14, which shows a marked decline in the temperature profile over time. At the pumping rate of 10^6 m^3/day, the geothermal gradient is incapable of replenishing the heat absorbed by the endothermic dissociation, and even the lower parts of the free gas zone begin to cool. This cooling (observed universally in simple depressurization processes of hydrates) tends to indicate that depressurization alone may not be a very effective method of gas production from hydrates because the resulting cooling shifts the equilibrium substantially. Temperature being a far more potent means of affecting dissociation than pressure, the continuous cooling slows dissociation. Note that the temperature drop does not advance deep into the hydrate because of their low conductivity.

The gas, hydrate and water saturations in Figures 15, 16 and 17, respectively, show that the hydrate layer begins to exhibit signs of deterioration late into the simulation (indicated by the lower saturation after 12 years of production), while the gas saturation shows very little increase over the same period. This is attributed to the continuous production (which removes gas from the system), to the release of large amounts of water during dissociation, and to the continuously declining gas release (due to cooling). The change in water saturation shows the effects of drainage after the dissociation of the hydrate, indicated by the downward movement of a high water saturation band.

Summary and Discussion

EOSHYDR2 is a new module for the TOUGH2 general-purpose simulator for three-dimensional, multi-component, multiphase fluid and heat flow and transport in the subsurface. EOSHYDR2 is designed to model the non-isothermal gas release, phase behavior and flow under the conditions of the common methane hydrate deposits (i.e., binary hydrates involving methane in the permafrost and in deep ocean sediments) by solving the coupled equations of mass and heat balance. The model can also describe hydrate behavior under extreme laboratory conditions. As with all other members of the TOUGH2 family of codes, EOSHYDR2 can handle multi-

dimensional flow domains and cartesian, cylindrical or irregular grids, as well as porous and fractured media.

EOSHYDR2 includes both an equilibrium and a kinetic model of hydrate formation and dissociation, and can describe hysteresis between the formation and dissociation equilibrium curves. The model accounts for up to four phases (gas phase, liquid phase, ice phase and hydrate phase) and up to nine components (CH_4-hydrate, water, native and dissociated methane, a second native and dissociated hydrocarbon, salt, water-soluble inhibitors and heat). The mass components are partitioned among the phases, and their thermophysical properties can be described at temperatures as low as –110 ^oC. Dissociation, phase changes and the corresponding thermal effects are fully described, as are the effects of salt and inhibitors. The model can describe all possible hydrate dissociation mechanisms, i.e., depressurization, thermal stimulation, salting-out effects and inhibitor-induced effects

Although EOSHYDR2 has the ability to model kinetically-controlled hydrate dissociation, only the equilibrium model was used in the four tests conducted in this study because of lack of the necessary parameters. The first test involved CH_4 production from a stratified reservoir of CH_4-hydrate and free CH_4 gas through a depressurization process under permafrost conditions with zero and non-zero initial gas saturation in the hydrate zone. The second test modeled depressurization-induced CH_4 production from a reservoir of CH_4-hydrate and salt water (uniformly distributed) under oceanic conditions. The third test modeled the thermal stimulation process of the frontal sweep system, which involved injection of hot water and hot brine to dissociate CH_4 in a CH_4-hydrate and water reservoir. The fourth test involved production from a suboceanic hydrate-capped gas reservoir with a domal structure, and studied the dissociation of a methane-ethane hydrate.

The results of the tests tend to indicate that CH_4 production from CH_4-hydrates is technically feasible and has significant potential. Both depressurization and thermal stimulation seem to be capable of producing substantial amounts of CH_4 gas, although thermal stimulation appears to have an advantage, and combination of the two in injection-production systems seems to be the most desirable approach. It is not possible, however, to render a definitive judgment on the relative advantages of the methods because of the dearth of information on the properties of hydrate reservoirs and their field thermodynamic behavior. There are practically no reliable measurements of the permeability, porosity and saturation of natural hydrate deposits, while the understanding of the kinetic behavior of hydrates is at a very early stage[1]. Additionally, there are significant scientific challenges and knowledge gaps that must be addressed for numerical simulation to provide reliable predictions of gas production. These include the type of formation/dissociation reactions occurring in natural accumulations (equilibrium vs. kinetic), the values and temperature dependence of the corresponding parameters under field conditions, the hysteretic behavior between the formation and dissociation P-T equilibrium curves, the relative permeability in hydrate formations, hydrocarbon solubility near the hydration point, hydrate thermal properties, and the effect of the hydration number on the properties and behavior of hydrates. The fact that no representative undisturbed sample of natural hydrates has been obtained to-date indicates the magnitude of the problem.

Thus, at this stage, our ability to describe mathematically the hydrate system exceeds our basic understanding and our ability to verify the codes. This should not be interpreted as lack of confidence in the role of numerical simulation. The enormity and potential of this resource clearly demands evaluation, and numerical studies are a powerful and efficient way to accomplish this. Even with the current lack of data, numerical simulation makes it possible to establish envelopes of possible solutions and to identify promising target zones of hydrates for development. Thus, the currently available data on hydrates allow the determination of the model sensitivity to inputs and the relative importance of the various reservoir and production parameters. However, data representative of reservoir conditions must be obtained to render models sufficiently robust for accurate predictive applications.

Nomenclature

A_κ = specific area of the particle of the κ-hydrate (m^2)
b = Klinkenberg factor (Pa)
C_R = heat capacity of dry rock ($J/kg/^0K$)
d = molecular diffusion coefficient (m^2/s)
$\mathbf{D}$ = hydrodynamic dispersion tensor (m^2/s)
ΔE = hydrate dissociation activation energy (J/kg)
f = fugacity (Pa)
$\mathbf{F}^\kappa$ = Darcy flux vector of component κ ($kg/m^2/s$ or W/m^2)
$\mathbf{g}$ = gravitational acceleration vector (m/s^2)
h = specific enthalpy (J/kg)
ΔH^0 = hydrate heat of dissociation (J/kg)
ΔH^f = heat of fusion of ice (J/kg)
$\mathbf{I}$ = unit vector
k = intrinsic permeability (m^2)
K = thermal conductivity ($W/m/^0K$)
k_κ = reaction constant of the kinetic dissociation of hydrate κ ($1/s^2$)
k_r = relative permeability (m^2)
K_d = sorption distribution coefficient (m^3/kg)
N, N_H = hydration number
$\mathbf{n}$ = inward unit normal vector
M^κ = mass or heat accumulation term of κ (kg/m^3 or J/m^3)
P = pressure (Pa)
P_c = capillary pressure (Pa)
q = mass or heat external generation rate κ ($kg/m^3/s$ or W/m^3)

q_d = rate of direct heat addition/removal (W/m^3)
Q = mass or heat internal generation rate due to dissociation (kg/m^3/s or W/m^3)
r = radius (m)
R = gas constant (=8.314 J/mol/^{0}K)
S = phase saturation
t = time (s)
T = temperature (^{0}K)
T_{fs} = freezing point of a salt solution (^{0}K)
u = specific internal energy (J/kg/^{0}K)
v = pore velocity (m/s)
$\mathbf{v}$ = pore velocity vector (m/s)
V_n = volume of subdomain n (m^3)
x,y,z = coordinates (m)
x = mole fraction in the aqueous phase
X = mass fraction
y = mole fraction in the water-free gas phase
Y = mole fraction in the gas phase
W = molecular weight (kg/mol)
Z = gas compressibility factor

Greek Symbols

α = dispersivity (m)
Γ_n = surface area of subdomain n (m^2)
ϕ = porosity
ρ = density (kg/m)
τ = tortuosity
χ = mole fraction of constituent hydrates in composite hydrate

Subscripts and Superscripts

A = aqueous phase
e = equilibrium
G = gas phase
H = solid hydrate phase
i = inhibitor component
I = solid ice phase
m = methane component
R = rock
s = salt component
w = water component
β = phase
κ = a component
ν = a hydrocarbon component other than methane
θ = heat pseudo-component

Acknowledgement

This work was supported by the Assistant Secretary for Fossil Energy, Office of Natural Gas and Petroleum Technology, through the National Energy Technology Laboratory, under the U.S. Department of Energy, Contract No. DE-AC03-76SF00098. The author is indebted to Stefan Finsterle and John Apps for their insightful review comments.

References

1. Sloan, E.D.: *Clathrate Hydrates of Natural Gases*, Marcel Dekker, Inc., New York, NY (1998)
2. McGuire, P.L.: "Methane Hydrate Gas Production: An Assessment of Conventional Production Technology as Applied to Hydrate Recovery, Report LA-9102-MS, Los Alamos National Laboratory, Los Alamos, NM (1981).
3. Holder, G.D., Angert, P.F., John, V.T., and Yen, S.L.: "Simulation of gas Production From a Reservoir Containing Both Gas Hydrates and Free Natural Gas", paper SPE 11105 presented at the 1982 SPE Meeting, New Orleans, LA, 26-29 September.
4. Kamath, V.A., and Godbole, S.P.: "Inhibitor-Induced Hydrate Dissociation", *J. Pet. Tech*. (1987), **39**, 1379.
5. Drenth, R.J.J., and Swinkels, W.A.M.: "A Thermal Reservoir Simulation Model for Natural Gas Hydrate Production", *Proc*., Intl. Symposium on Methane Hydrates, organized by JNOC, Chiba (October 1988).
6. Swinkels, W.A.M., and Drenth, R.J.J.: "Thermal Reservoir Simulation Model of Production From Naturally Occurring Gas Hydrate Accumulations", *SPERE* (2000), **3**(6), 559.
7. Moridis, G.J.: "EOSHYDR: A TOUGH2 Module for CH4-Hydrate Release and Flow In the Subsurface", Report LBNL-42386, Lawrence Berkeley Laboratory, Berkeley, CA (1998).
8. Pruess, K.: "TOUGH2 - A general purpose numerical simulator for multiphase fluid and heat flow", Report LBL-29400, Lawrence Berkeley Laboratory, Berkeley, CA (1991).
9. Pruess, K., C. Oldenburg, and Moridis, G.: "TOUGH2 User's Guide – Version 2.0", Report LBL-43134, Lawrence Berkeley Laboratory, Berkeley, CA (1999).
10. Nielsen, R. B., and Bucklin, R.W.: "Alcohol Effects on Hydrate Dissociation", *Hydrocarbon Processing*, 71 (April 1983).
11. Millington, R. J., and Quirk, J.P.: "Permeability of Porous Solids", *Trans. Faraday Soc.* (1961), **57**, 1200.
12. Kim, H.C., Bishnoi, P.R., Heidemann, R.A., and Rizvi, S.S.H.: "Kinetics of Methane Hydrate Decomposition", *Chem. Eng. Sci*. (1987), **42**(7), 1645.
13. Clarke, M.A., and Bishnoi, P.R.: "Determination of the Intrinsic Rate of Ethane Gas Hydrate Decomposition", *Chem. Eng. Sci.* (2000), **55**, 4869
14. Clarke, M.A., and Bishnoi, P.R.: "Determination of the Activation Energy and Intrinsic Rate Constant of Methane Gas Hydrate Decomposition", *Can. J. Chem. Eng.* (2001), **79**(1), 143.
15. Kamath, V.A..: "Study of heat transfer characteristics during dissociation of gas hydrates in porous media", Ph.D. dissertation, Univ. of Pittsburgh., Pittsburgh, PA (1984).
16. Carson, D.B., and Katz, D.L.: "The Distribution Coefficient Method to Determine Hydrate Composition", *Trans. AIME.* (1942), **146**, 150.
17. Soreide, I., and Whitson, C.H.: "Peng-Robinson Predictions for Hydrocarbons, CO_2, N_2, and H_2S With Pure Water and NaCl Brine", *Fluid Phase Equil*. (1992), **77**, 217.

18. Vargaftik, N.B.: *Tables on the Thermophysical Properties of Liquids and Gases*, John Wiley and Sons, New York, NY (1975).
19. Kobayashi, R., and Katz, D.L.: "P-T-X Diagrams of Methane-Water Systems", *Trans. AIME* (1949), **186**, 66.
20. Chung, T.-H., Ajlan, M., Lee, L.L., and Starling, K.E.:"Viscosity of Real Gases", *Ind. Eng. Chem. Res.* (1988), **27**, 671.
21. Parker, J.C., Lenhard, R.J., and Kuppusamy, T.: "A Parametric Model for Constitutive Properties Governing Multiphase Flow in Porous Media", *Water Resour. Res.* (1976), **12**(1), 57.

Table 1 – Reservoir Properties	
Parameter	**Value**
Gas zone thickness	50 m
Hydrate zone thickness	50 m
Initial pressure	2.05×10^7 Pa
Initial temperature	293.3 K
Gas composition	100% CH_4
Permeability	4.325×10^{-14} m^2
Gas production rate	0.82 m^2/s
Thermal conductivity	1.5 W/m/K
Thermal diffusivity	7×10^{-7} m^2/s

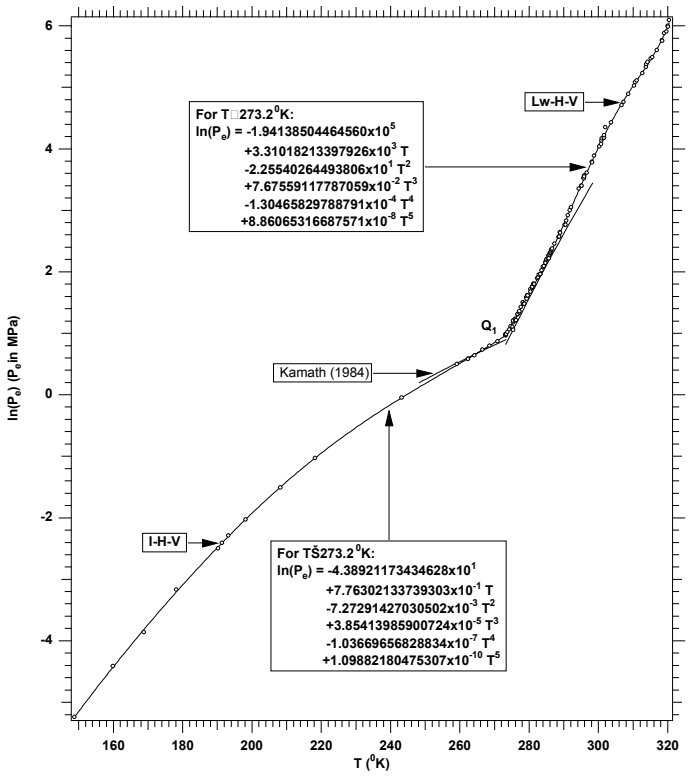

Figure 1 – Pressure-temperature equilibrium of the simple methane hydrate.

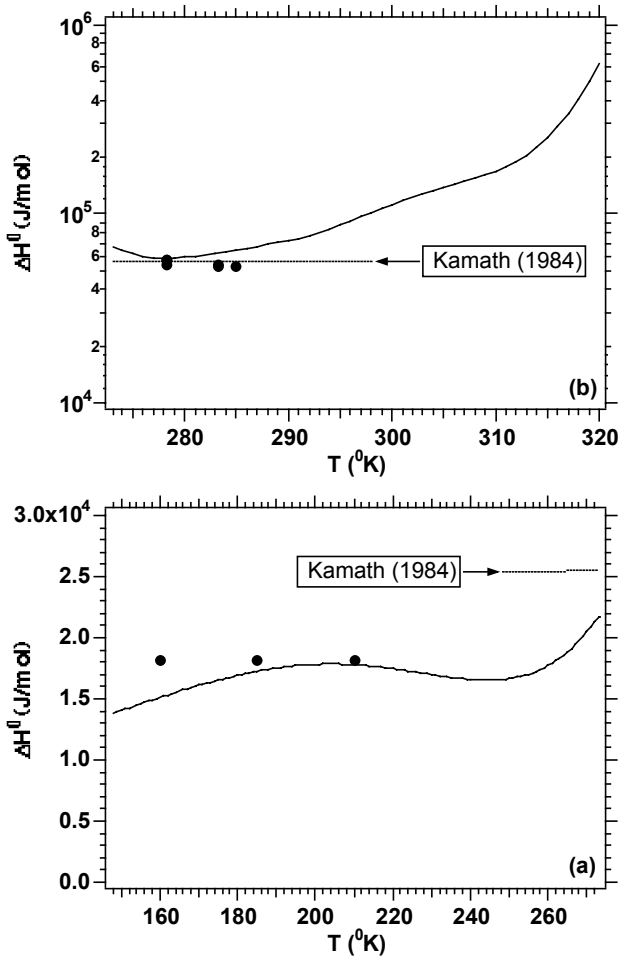

Figure 2 – Temperature dependence of the enthalpy of dissociation for the I-H-V (a) and Lw-H-V (b) systems.

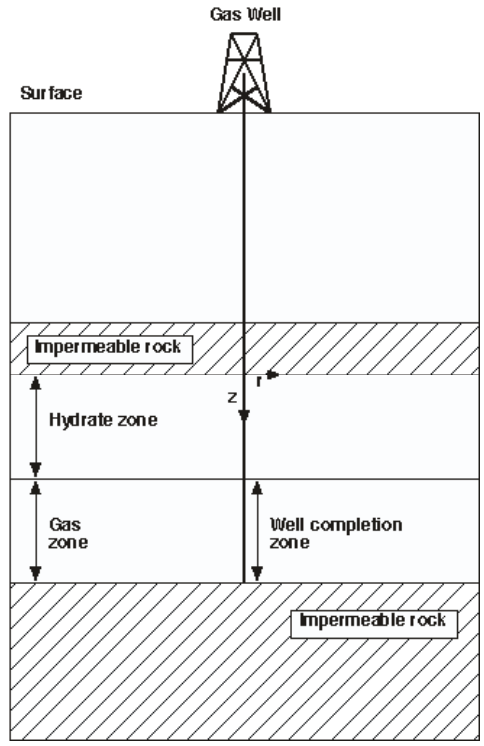

Figure 3 - The reservoir configuration in Test Problem 1.

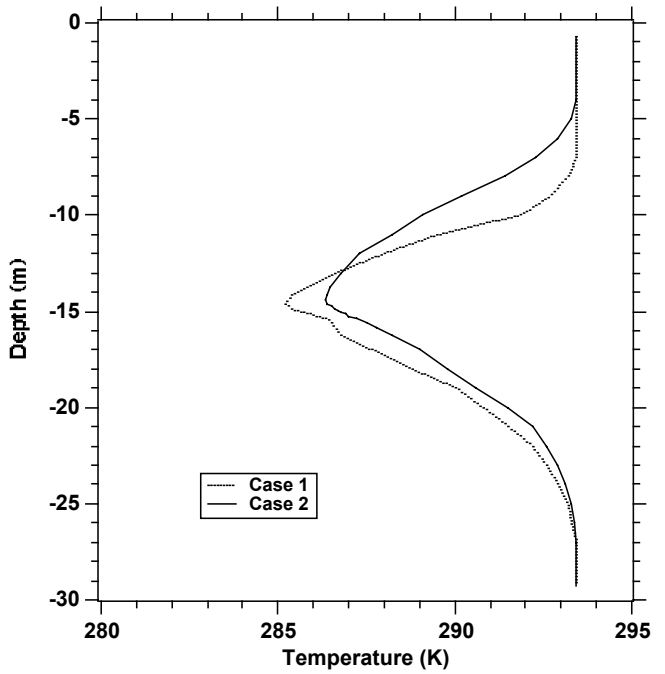

Figure 5 - Vertical temperature distribution at r=0.15 m in Test Problem 1.

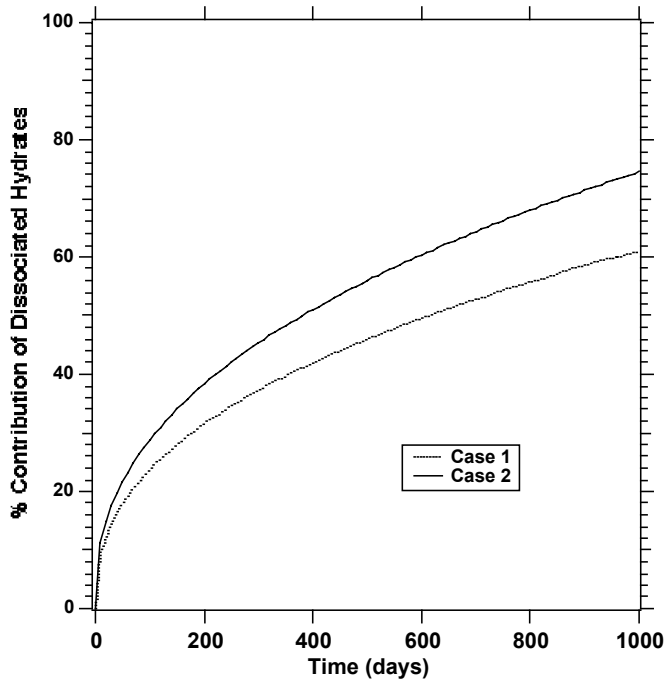

Figure 4 - Cumulative contribution of CH_4 dissociated from hydrates to the total gas production in Test Problem 1.

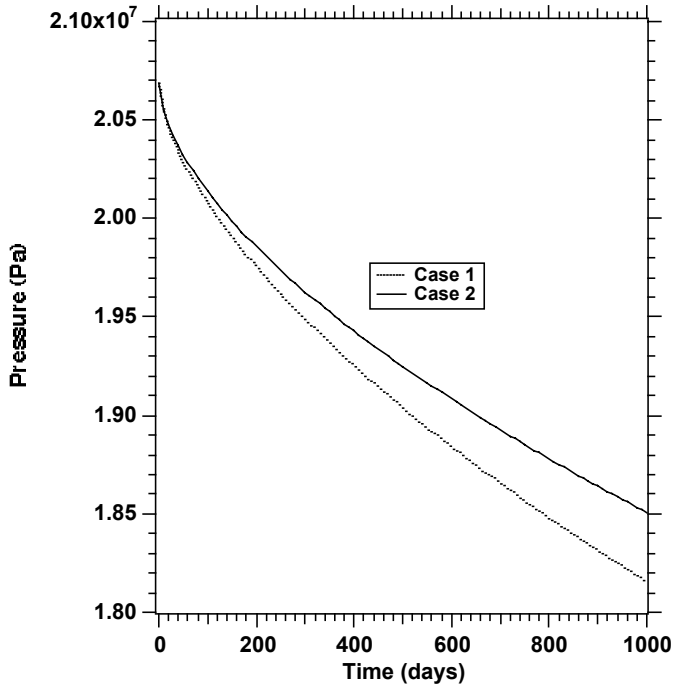

Figure 6 - Pressure vs. time at the wellbore gridblock located at r=0.05 m, z=-15.05 m.

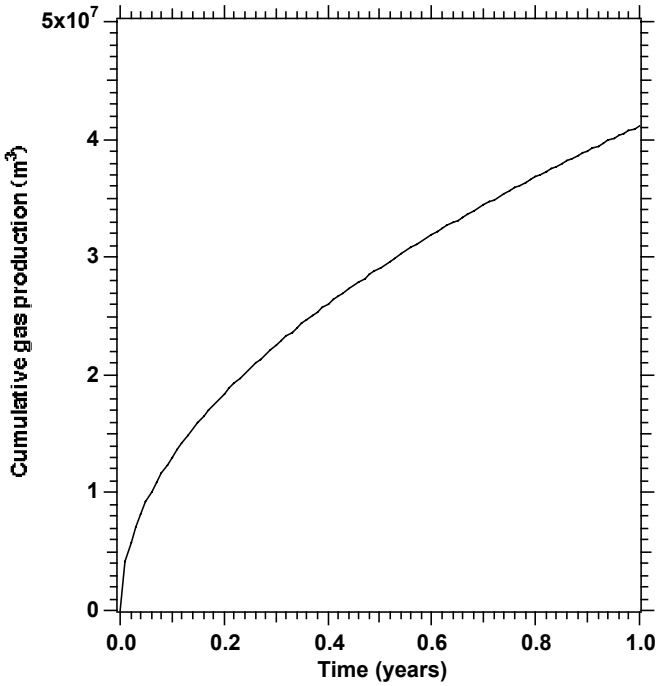

Figure 7 - Cumulative CH_4 production at = 1 year in Test Problem 2.

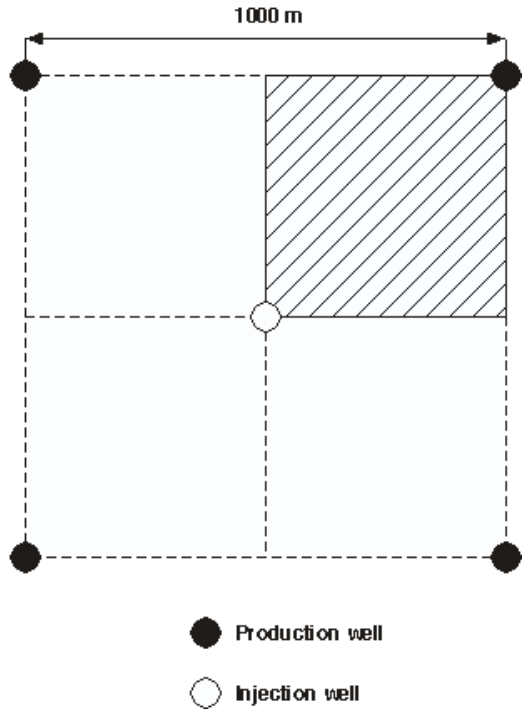

Figure 9 - Five-spot well pattern for modeling a 1/4 symmetry subdomain in the frontal sweep problem.

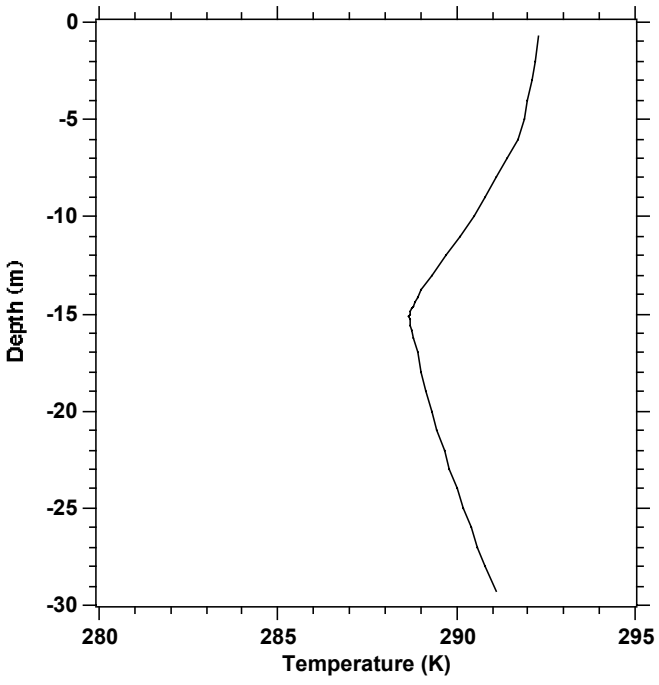

Figure 8 - Vertical temperature distribution at r=0.15 m in Test Problem 2.

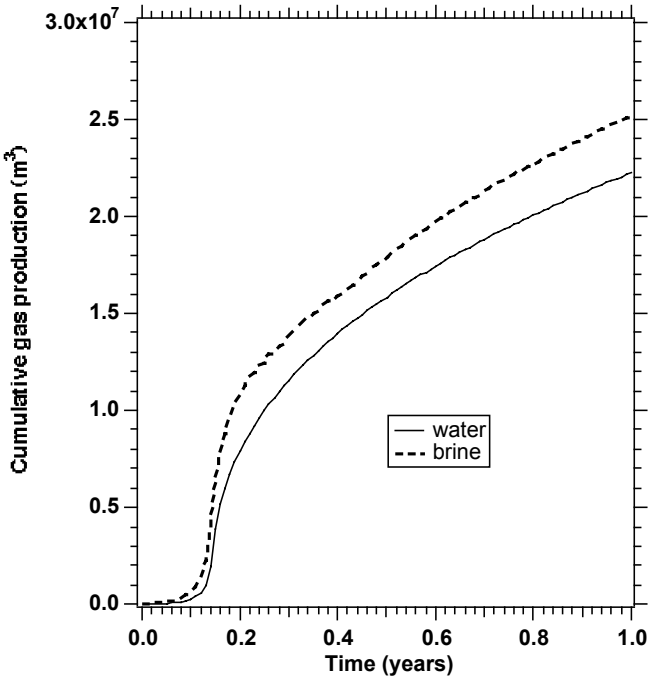

Figure 10- Cumulative CH_4 production at t=1 yr in Test Problem 3.

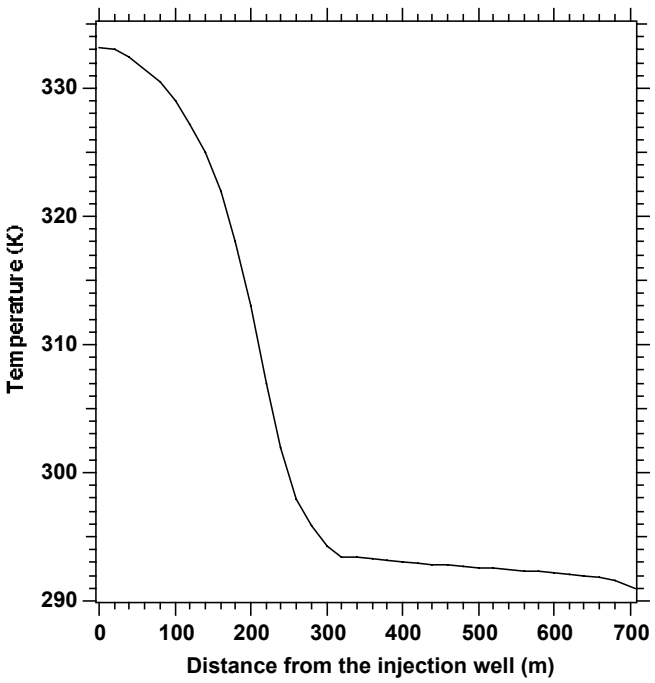

Figure 11- Temperature distribution at t= 1 year and at z = -16.03 m along the axis connecting the injection and the production wells in Problem 3.

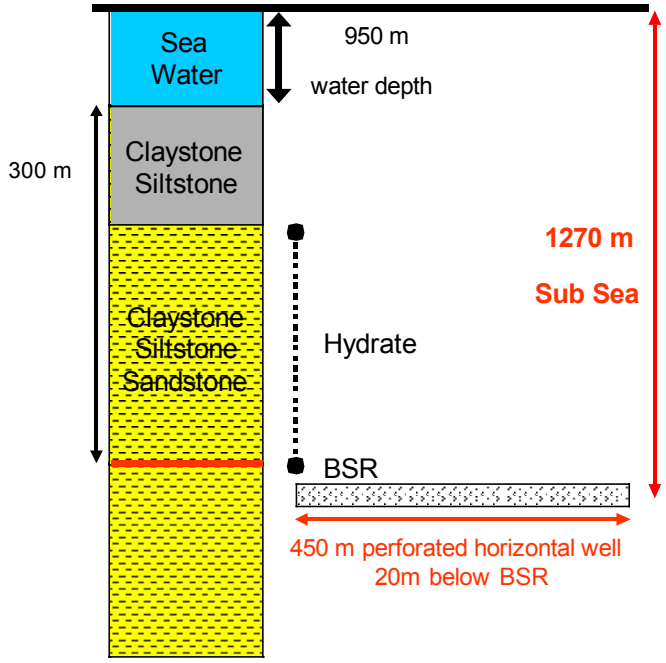

Figure 12- Schematic of the reservoir location and geology in the suboceanic reservoir of test Problem 4 (from Drenth and Swinkels, personal communication).

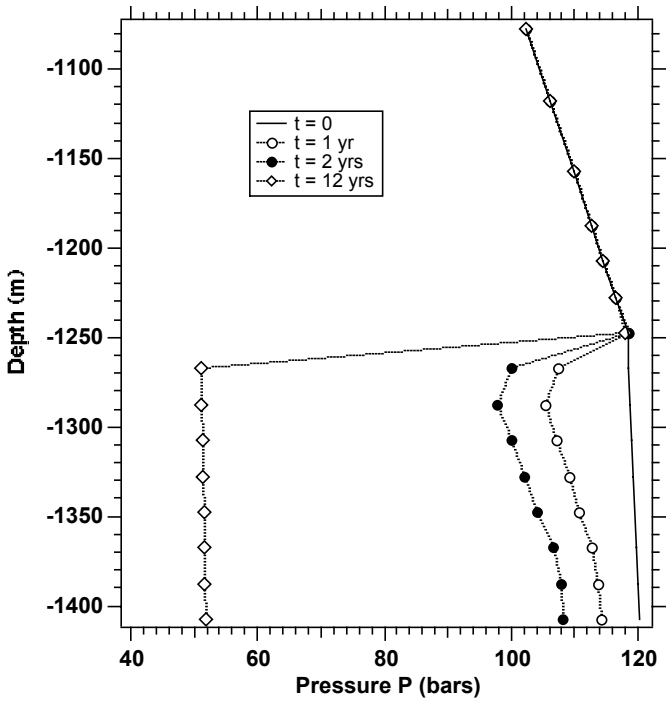

Figure 13- Pressure distribution in the reservoir of Problem 4.

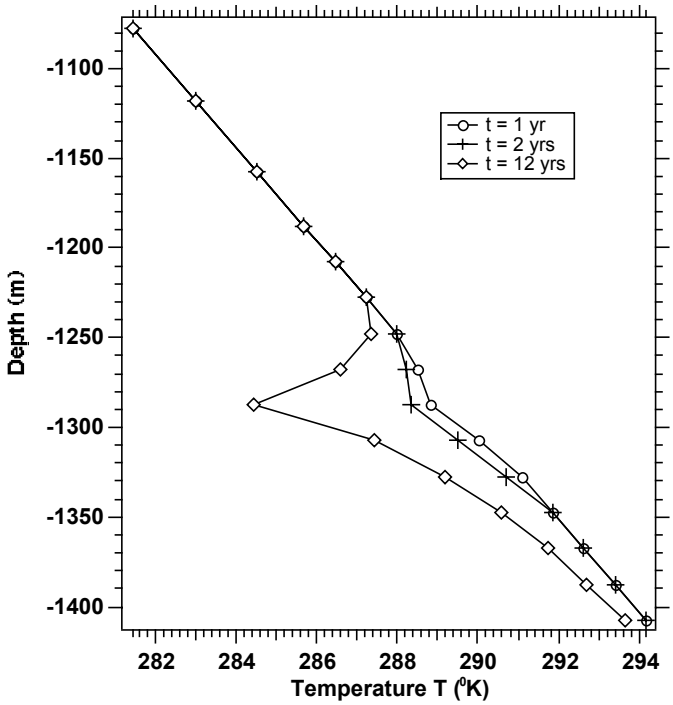

Figure 14- Temperature distribution in the reservoir of Problem 4.

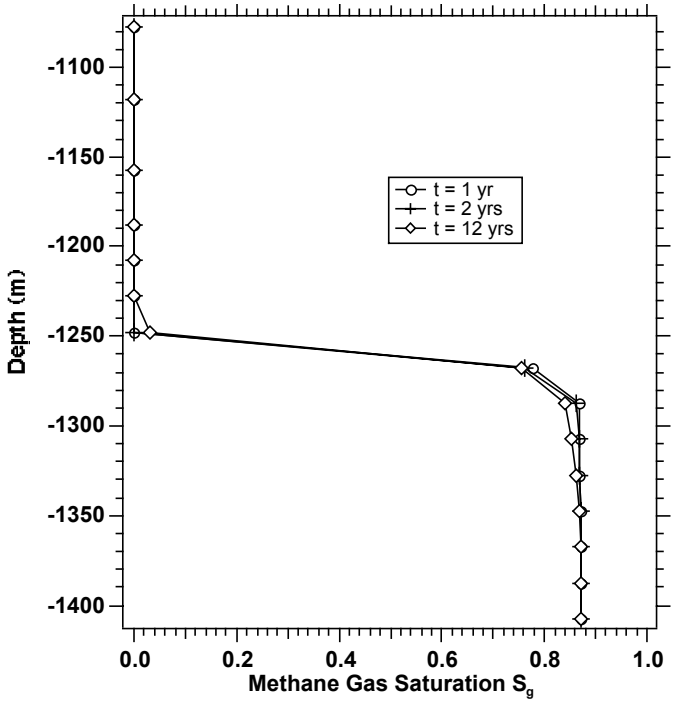

Figure 15 - Gas saturation distribution in the reservoir of Problem 4.

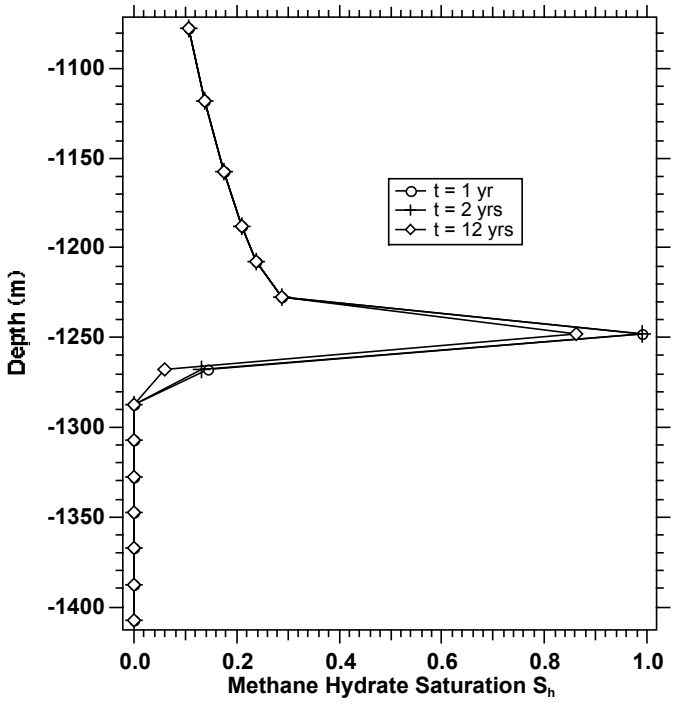

Figure 16 - Hydrate saturation distribution in the reservoir of Problem 4.

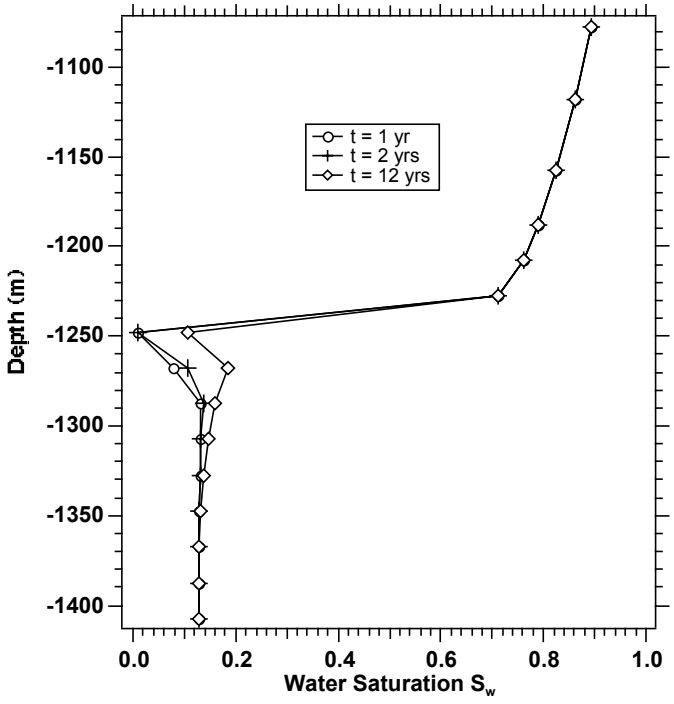

Figure 17- Water saturation distribution in the reservoir of Problem 4.